scientific reports

Check for updates

OPEN

Analysis of raltegravir analogs to enhance inhibitory efficiency against HIV integrase

Hanieh Sabaghian & Mehdi Yoosefian✉

This article addresses the improvement of the efficacy of anti-integrase enzyme drugs for the AIDS virus, especially using the drug Raltegravir and its 21 analogs. In this research, Hartree-Fock and Density Functional Theory methods have been employed for the design and optimization of new drug candidates. These methods are used to enhance the accuracy and reactivity of the drugs. Additionally, docking is used to investigate the interactions between the drug and the target and evaluate binding energies. Molecular dynamics simulation is utilized to validate binding results. Computational results indicate that the designed analogs exhibit higher reactivity. In molecular docking calculations, RAL5 and RAL21 show the best binding energies of -10.10 and −10.92 kcal/mol, respectively, indicating their superior efficiency. The analysis of inhibitor potentials against the HIV-1 integrase enzyme through molecular dynamics simulation reveals that RAL5 has strong inhibitory potential for treating viral diseases. These findings contribute to the promotion of therapeutic intervention methods in this field.

Keywords HIV-1 integrase, Drug design, Viral disease treatment, Raltegravir

Technological advancements in pharmaceutical research have catalyzed a paradigm shift in drug design methodologies, particularly through the integration of computational tools. This convergence of computational prowess and medical science has not only expedited the drug discovery process but has also led to the development of targeted therapeutic strategies[1–4]. Targeted drug design, focusing on specific molecular targets, has emerged as a specialized aspect of this methodology, particularly notable in the case of HIV-1, the virus responsible for AIDS[5]. Understanding and neutralizing key viral components, such as integrase, has become paramount in developing effective antiretroviral therapies[6]. HIV-1 integrase (HIV-IN), a crucial enzyme facilitating the integration of viral DNA into the host genome, has become a focal point for drug design efforts. Integrase inhibitors, a novel class of antiretroviral drugs, work by impeding this integration process, thereby hindering virus replication independently of other antiretroviral drugs[7]. The integration of the host genome is one of the important steps in the replication of this virus, which is performed by the integrase enzyme and the host cell enzyme. This enzyme has a spatial structure with three domains[8]. For its function, the integrase protein must interact with other viral components, such as matrix proteins and protein R. This interaction forms a complex called the pre-integration complex[9]. The integration stage is one of the vital phases in the HIV life cycle[10]. Integrase inhibitors are a new class of antiretroviral drugs that inhibit the integration process, preventing virus replication. By blocking the integration of HIV DNA into the host cell DNA, integrase inhibitors prevent virus replication[11–13].

Among the HIV-IN inhibitors, Raltegravir (RAL) stands out as the first-in-class drug that has demonstrated potent activity against various strains of HIV-1, including those resistant to other antiretroviral therapies[14,15]. Structurally, RAL contains a unique beta-hydroxyketone motif, which is believed to confer its inhibitory activity by binding to divalent metals at the HIV-IN active site. This mechanism of action effectively prevents the integration of viral DNA into the host genome, thereby halting viral replication[16,17]. Clinical trials have demonstrated the efficacy of RAL, particularly in patients who have failed current treatments[18]. However, ongoing research in computational drug design holds promise for developing newer drug candidates with enhanced efficacy and safety profiles. Structure-based drug design, employing techniques like quantum mechanics, molecular docking and molecular dynamics simulation, enables the design and evaluation of these analogs. Molecular docking studies facilitate the screening of large compound libraries to identify molecules with favorable binding affinities and interactions with the target protein[19]. By computationally simulating the binding process, researchers can prioritize compounds with the potential to inhibit HIV-IN activity effectively. Moreover, molecular dynamics simulations provide a dynamic view of the drug-protein interactions, allowing

Department of Chemistry, Graduate University of Advanced Technology, Kerman, Iran. ✉email: myoosefian7@gmail.com

researchers to explore the conformational changes and structural dynamics of the protein-ligand complex over time. This dynamic perspective offers valuable insights into the stability and binding kinetics of the drug candidate, aiding in the selection of lead compounds for further experimental validation[20–22]. In the quest for improved integrase inhibitors, computational methods also play a crucial role in the rational design of novel drug analogs with enhanced potency and specificity[19]. Furthermore, computational approaches enable the exploration of drug resistance mechanisms and the design of strategies to overcome resistance mutations, ensuring the long-term effectiveness of antiretroviral therapies[21,23]. By studying the molecular mechanisms underlying drug resistance, researchers can design inhibitors that target al.ternative binding sites or exhibit a higher barrier to resistance[22,24]. The ultimate goal of this study is to design and optimize new analogs of the drug Raltegravir by utilizing modern structure-based drug design (SBDD) approaches, aiming to enhance the inhibitory efficiency against the HIV-1 integrase enzyme. In this regard, quantum mechanical calculations (DFT and Hartree-Fock) were employed to investigate reactivity indices and electronic properties; molecular docking studies were used to evaluate binding energies and key interactions; and molecular dynamics simulations were conducted to analyze the structural stability of drug–enzyme complexes under physiological conditions. In addition, all analogs were thoroughly evaluated for pharmacokinetic properties, toxicity, blood-brain barrier permeability, bioavailability, systemic stability, and drug-likeness based on rational drug design principles. The results indicate that some of the designed analogs, particularly RAL5 and RAL21, not only exhibit lower binding energies and higher reactivity, but also possess favorable pharmacokinetic properties and synthetic feasibility. Therefore, they can be considered strong candidates for the development of next-generation anti-HIV drugs. This research represents a significant step toward the design of more targeted and effective therapies for patients living with HIV/AIDS.

Materials and methods

Preparation of protein

The three-dimensional structure of the HIV-IN is accessible through the RCSB Protein Data Bank[25]. This structure is available in the database with the identifier 7RQ0. The protein's structure has been determined using X-ray crystallography, with a resolution of 1.95 Å. To utilize protein crystal structures, receptor binding compounds and solvent molecules have been removed. Subsequently, necessary corrections were applied to the receptor using the Chimera software, and the structure was optimized using Dock Prep and the AMBER ff14SB force field. The optimized structure was then saved in PDB format, which is the preferred input format for AutoDock. This format is suitable for molecular interaction studies and molecular simulations.

Preparation of ligand

The structure of RAL (Raltegravir) was retrieved from the PubChem database, drawn using ChemBioDraw Ultra 14.0, and converted to three-dimensional coordinates in the ChemBio3D Ultra 14.0 environment. Then, its molecular geometry was optimized using the minimum energy method in Chimera software and the AMBER ff14SB force field, and the final structure was saved in PDB format for use in subsequent steps[26,27]. Next, using GaussView 0.6 software, 21 new analogs of RAL were designed with the aim of improving drug performance and increasing stability and interaction with the HIV-1 integrase enzyme. In designing these analogs, modifications such as substituting functional groups, adding heterocyclic or aromatic rings, and altering the positions of polar groups were applied. In RAL1, the 1,3,4-oxadiazole ring was converted to a 4 H-1,2,4-triazole, which improved hydrogen bonding capacity and consequently enhanced the binding affinity of the molecule with the target enzyme. RAL2 involved replacing the carboxylic acid group with a nitrile group, which increased lipophilicity and metabolic stability, thus potentially prolonging the compound's half-life. RAL3 included an additional pyridine ring in the side chain, promoting π-π interactions with aromatic residues in the active site and improving molecular recognition. In RAL4, the introduction of heterocyclic rings containing nitrogen and oxygen atoms contributed to increased polarity and enhanced aqueous solubility, as well as improved binding through polar interactions. RAL5 contained an isoindole ring and a fluorine atom; the fluorine improved membrane permeability and metabolic resistance, while the isoindole provided favorable steric interactions within the binding pocket. RAL6, featuring two nitrile groups and an imidazole ring, showed enhanced lipophilicity, stronger electronic interactions, and improved potential for metal ion coordination with the active site. The addition of amino and chlorine groups in RAL7 led to increased hydrogen bonding potential and enhanced lipophilicity, which can facilitate better cell permeability. In RAL8, the presence of an extra aromatic ring and multiple carboxylic groups improved both π-stacking and ionic interactions with charged residues, enhancing overall binding strength. RAL9 was modified with several amino groups and a new side ring, which collectively increased conformational flexibility and promoted additional hydrogen bonding. RAL10 incorporated a nitrile group at a new position along with a rearrangement of polar groups, optimizing the molecule's dipole moment and electrostatic interactions. In RAL11, the substitution of the indole structure enhanced aromatic interactions and improved molecular stability. RAL12 featured a bulkier chain, contributing to better steric complementarity and tighter fit within the enzyme's active site, increasing specificity. RAL13 included both triazole and pyrazine rings along with a longer chain, which improved hydrogen bonding, π-π stacking, and allowed better spatial reach to interact with deeper pockets of the enzyme. RAL14 introduced a nitrile group and a nitrogen-rich ring, providing opportunities for polar interactions and potential chelation with metal ions critical to enzyme function. In RAL15, the inclusion of additional amide and hydroxyl groups significantly enhanced hydrogen bonding and improved aqueous solubility. RAL16's longer chain and repositioned polar groups offered greater flexibility and adaptability in binding different conformations of the enzyme. The triazole and nitrile moieties in RAL17 contributed to improved metabolic stability and hydrogen bonding, supporting stronger and more selective binding. RAL18 contained an aromatic ring and multiple hydroxyl groups, enhancing both solubility and polar interactions with the target. RAL19 was characterized by the inclusion of several amide and carboxylic acid groups, which substantially increased hydrogen bond formation and electrostatic interactions. RAL20

incorporated more amide groups into a compact structure, improving conformational rigidity and interaction specificity. Finally, RAL21 was designed with an extended and flexible chain as well as repositioned polar groups, enabling better adaptation to the enzyme's binding site and dynamic interaction potential. After the design stage, all analogs were optimized and electronically analyzed using Gaussian 09 software at the DFT and Hartree-Fock theoretical levels to prepare them for the next steps, including docking and molecular dynamics simulations[28].

Designing and optimization of ligands

Gaussian 16[29] was used to perform Hartree-Fock and DFT/B3LYP calculations using the 6-311G basis set. Investigations of Frontier Molecular Orbital (FMO), Molecular Electrostatic Potential (MEP), and chemical descriptors were all conducted at the same theoretical level. The Gauss View 0.6 software was utilized for visualizing three-dimensional structures and calculating atomic charges, electronic density, and the optimized structure of 21 analogs. The hardness, softness, chemical potential and electrophilicity index of all compounds were calculated based on the energies of highest occupied molecular orbital (HOMO) and lowest unoccupied molecular orbital (LUMO), considering the Parr and Pearson's interpretation, the DFT theorem, and Koopmans' theorem.

Molecular docking study

Docking studies were conducted as part of the validation of the similarity prediction model. A model with over 97.4% remaining amino acid percentage in the allowed region of the Ramachandran plot was utilized for further screening. Hypothetical binding sites in the 7RQ0 model were identified using the PockDrug server[30]. Molecular docking was performed using AutoDock software version 1.5.2.4. The grid box, generated with AutoDock Tools, had dimensions (xyz) = (80, 80, 80) Å and a grid spacing of 0.375 Å[31]. The Lamarckian Genetic Algorithm (LGA) was employed as the search process for ligand binding and other parameters, using default settings in AutoDock Tools[32,33]. The three-dimensional structure of the protein was predicted, and ligand structures were converted to PDBQT format for further analysis. Flexible ligand binding simulations were performed with 250 runs and the genetic algorithm for evaluating binding energies. Hydrogen bonds, water-mediated interactions between HIV-IN and drugs, as well as the optimal interactions between protein-ligand complexes, were analyzed using molecular graphics tools such as LigPlot + and PyMol[34,35].

Molecular dynamics simulations (MDSs)

Molecular dynamics calculations provide better insights into the stability of ligand compounds identified by molecular docking. In this study, the 2022 version of the Gromacs software was used for molecular dynamics simulations. A topology file containing the ligands RAL, RAL5, and RAL21 along with the HIV-IN was created using CGenFF and then generated using the pdb2 gmx script with the Charmm36 force field[36]. Molecular dynamics simulations under periodic boundary conditions were performed using the Berendsen coupling algorithm, V-Rescale thermostat, and a Newtonian leap-frog integrator. To neutralize the system, 4 chloride ions and TIP3P water molecules were added to create a solvent[37–39]. The protein-ligand complex was equilibrated using the NVT ensemble (constant Number of particles, Volume, and Temperature) and the standard NPT ensemble (constant Number of particles, Pressure, and Temperature) at a temperature of 300 K and pressure of 1 atm. Finally, dynamic simulations were run for 250 ns.

Prediction of pharmacokinetic and drug-likeness properties

To evaluate the pharmacokinetic properties, toxicity, and drug-likeness of the designed compounds, all analogs, along with the reference drug Raltegravir (RAL), were analyzed using the online platform ADMETlab 2.0[40]. In this assessment, key parameters such as molecular weight, LogP, topological polar surface area (TPSA), plasma protein binding (PPB), blood–brain barrier (BBB) penetration, biological half-life, and synthetic accessibility score (SA score) were calculated for each compound. Furthermore, the compliance of the analogs with established drug design principles including Lipinski's Rule of Five and Pfizer's rule for minimizing toxicity was also examined.

Binding free energy calculations

The binding free energy can be calculated using methods such as Free Energy Perturbation, Bennett's Acceptance Ratio, and thermodynamic integration[41,42]. In this study, we used the molecular mechanics/Poisson Boltzmann surface area (MM-PBSA) methodology implemented in the g_mmpbsa tool of GROMACS[43] to calculate the binding free energies between the complexes HIV-IN/RAL, HIV-IN/RAL5 and HIV-IN/RAL21. In MM-PBSA, the binding free energy of the protein and ligand is regularly calculated by:

$$\triangle \mathrm{G}_{binding} = \triangle \mathrm{G}_{complex} = (\triangle \mathrm{G}_{protein} = \triangle \mathrm{G}_{ligand}) \tag{1}$$

The free energies of the protein-ligand complex, the protein, and the ligand are calculated separately in the solvent[44]. The overall free energy is defined as:

$$\mathrm{G} = \mathrm{E}_{\mathrm{MM}} + \mathrm{G}_{solvation} - \mathrm{TS} \tag{2}$$

E_{MM} represents the average molecular mechanics potential energy in a vacuum, while $\mathrm{G}_{\mathrm{solvation}}$ indicates the free energy of solvation. TS represents the entropic contribution to the free energy in a vacuum, with T and S denoting temperature and entropy, respectively. Additionally, E_{MM} consists of bonded and nonbonded terms, including bond angle, torsion, and electrostatic ($\mathrm{E}_{\mathrm{elec}}$) and van der Waals ($\mathrm{E}_{\mathrm{vdw}}$) interactions. Finally, the solvation free energy $\mathrm{G}_{\mathrm{solvation}}$ takes into account both electrostatic and non-electrostatic ($\mathrm{G}_{\mathrm{polar}}$ and $\mathrm{G}_{\mathrm{nonpolar}}$) components.

Properties	Residues	Percentage (%)
Residues in most favoured regions	228	97.40%
Residues in additional allowed regions	6	2.60%
Residues in generously allowed regions	0	0.00%
Residues in disallowed regions	0	0.00%
Number of non-glycine and non-proline residues	234	100.00%
Number of end-residues (excl. Gly and Pro)	12	
Number of glycine residues (shown as triangles)	24	
Number of proline residues	7	
Total number of residues	227	

Table 1. Ramachandran plot statistics showing residues present in favored and disallowed regions of the protein structure of 7RQ0.

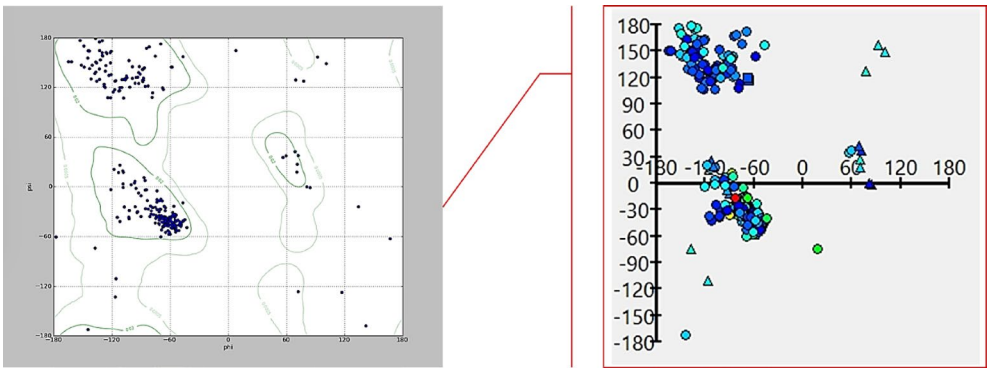

Fig. 1. Ramachandran diagrams of the 7RQ0 protein structure describing the favored and disallowed cases.

Gibbs free energy landscape (FEL) analysis

The results of the Principal Component Analysis (PCA) were analyzed using the Gibbs Free Energy Landscape (FEL) analysis. The Free Energy Landscape (FEL) is utilized for sampling three-dimensional structural data. FEL was generated in PyMOL using the "geo-measure" tool. The command gmx_sham was employed to create the 3D FEL to calculate the joint probability distribution in three-dimensional space[45].

Result and discussion

Reliability of protein structure and grid generation

The PROCHECK server was employed to assess and validate the quality and utility of the three-dimensional structure of the target protein. The PROCHECK and PyMol servers were used to generate a Ramachandran plot illustrating the allowed and disallowed regions of the protein backbone dihedral angles. A crucial criterion for a high-quality model is having over 90% of residues in favored regions. The stereochemical quality of the three-dimensional protein structure minimizes spatial interactions in the forbidden psi and phi angles. Table 1; Fig. 1 demonstrate that 97.4% of the residues reside in the most favorable region, 2.60% in the allowed region, and only 0.00% in the forbidden region of the prepared three-dimensional structure of the target protein (PDB ID: 7RQ0). After selecting the crystalline ligand of the target protein, the predicted active site was identified. The protein receptor grid was generated uniformly with its crystalline ligands. This identification enables the development of highly effective protein inhibitors through their binding sites.

Molecular geometry analysis

The molecular interactions between ligands and target proteins, crucial for various pharmaceutical activities, directly depend on the structural characteristics of the molecules. Density Functional Theory (DFT) and Hartree-Fock calculations using the 6-311G basis set provide information about electronic effects and charge transfers in ligand-protein interactions. Optimized two-dimensional structures along with calculated parameters in Fig. 2; Table 2 are presented. In other words, these calculations encompass the description of HOMO and LUMO energies, reactivity, shape, properties of a complete molecule's bonding, as well as molecular fragments and substitutions. Recently, the successful application of the HOMO and LUMO concepts has been evident in explaining the biological activities and molecular properties of drug candidates.

Molecular orbital analysis and molecular electrostatic potential analysis

The energy separation between frontier molecular orbitals, constituting the gap between HOMO and LUMO, reflects the dynamical stability and chemical reactivity of a molecule. The HOMO-LUMO energy gaps for RAL

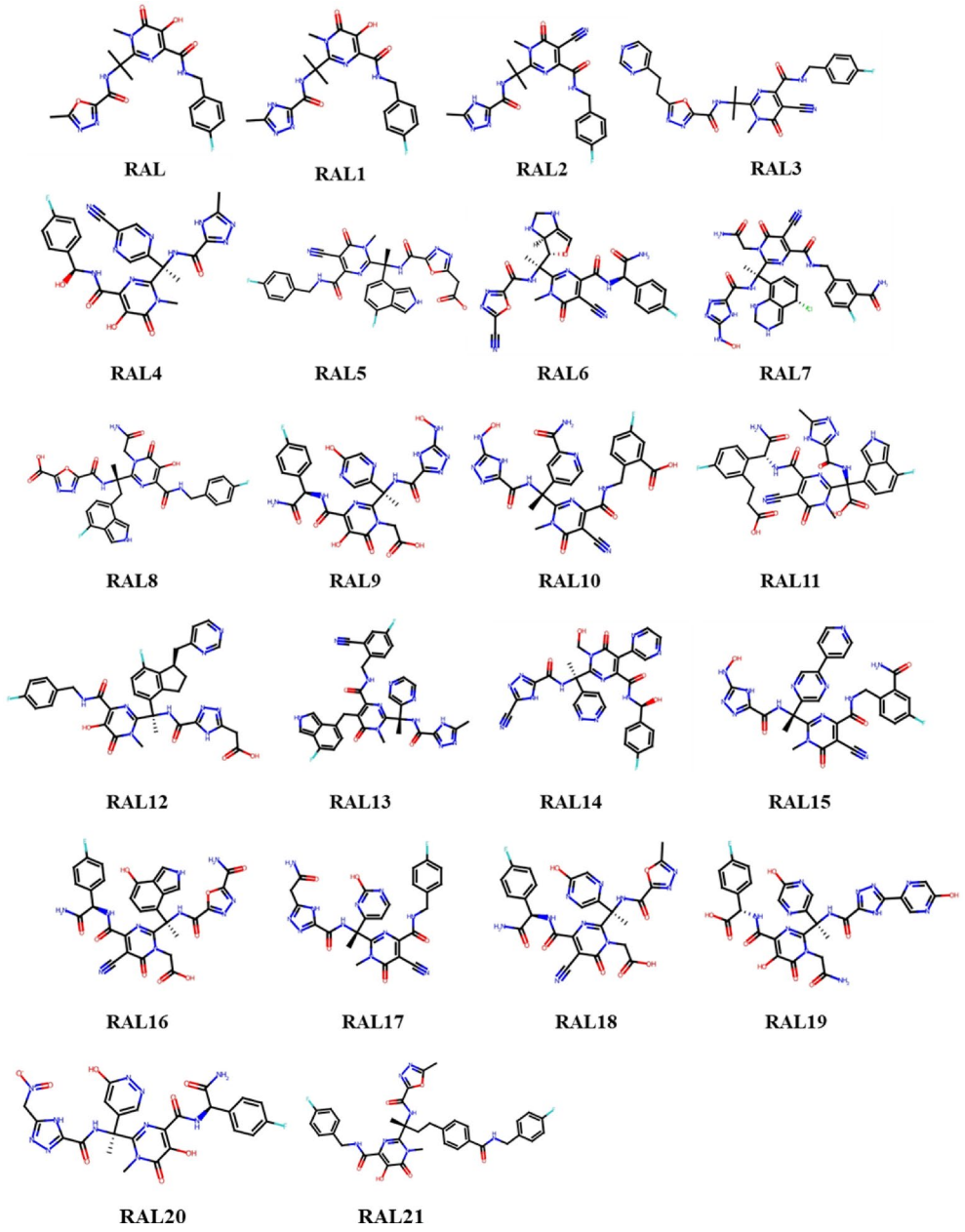

Fig. 2. Optimized 2D structure of Raltegravir (RAL) drug and new designed analogs.

and the designed analogs were calculated at the DFT/B3LYP levels using the 6-311G basis set, and the graphical representation of these orbitals is depicted in Fig. 3A. The positive and negative phases of molecular orbitals can be discerned in red and green, respectively. The color-coded examination of HOMO and LUMO orbitals reveals the electron density transition path from ground to excited states. Both are considered key orbitals playing roles in chemical reactivity and biological activity. According to Koopmans' theorem, the ionization potential (I) and electron affinity (EA) of RAL can be expressed through the HOMO and LUMO energies as follows:

I = −6.44 eV and EA = −2.19 eV and the HOMO-LUMO gap = 4.25 eV; Based on this, chemical potential, μ=−4.31 eV and hardness, η =−2.12 eV were computed (see Table 3). A large HOMO/LUMO energy gap is associated with a hard molecule, while a small HOMO/LUMO gap is associated with a soft molecule. Therefore, a molecule with a smaller HOMO/LUMO gap is expected to be more reactive. Electrophilicity index (ω) of RAL was calculated by implementing the formula of as $\omega = \frac{\mu^2}{2\eta} = 4.38$ eV, which defines a quantitative classification of global electrophilic nature of a compound. They anticipated ω as a measure of energy lowering due to maximal electron flow between donor and acceptor. As shown in Table 3, it is evident that the RAL analogs, RAL5, and RAL21, exhibit lower HOMO-LUMO gaps and higher softness, which may contribute to their chemical reactivity and polarity compared to RAL. Furthermore, Molecular Electrostatic Potential (MEP) for predicting reactive sites for electrophilic and nucleophilic attacks, were calculated and presented in Fig. 3B. The red color

Compound	ET(HF)	ET(DFT)	Dipole moment (Debye)
RAL	−1563.07	−1579.15	176.79
RAL1	−1541.62	−1559.32	166.6
RAL2	−1558.38	−1576.32	265.4
RAL3	−1876.95	−1898.56	328.04
RAL4	−1928.5	−1950.53	196.83
RAL5	−2182.41	−2207.21	381.56
RAL6	−2131.66	−2155.94	384.76
RAL7	−2811.97	−2841.81	191.68
RAL8	−2332.48	−2358.9	76.9
RAL9	−2279.76	−2305.49	116.83
RAL10	−2206.18	−2231.24	285.31
RAL11	−2554.94	−2583.93	322.21
RAL12	−2428.91	−2456.72	183.61
RAL13	−2275.04	−2301.25	176.4
RAL14	−2149.65	−2174.24	126.19
RAL15	−2279.66	−2305.78	145.99
RAL16	−2453.39	−2481.25	380.74
RAL17	−2020.93	−2044.02	317.2
RAL18	−2227.16	−2252.39	308.11
RAL19	−2486.37	−2514.55	93.36
RAL20	−2206.38	−2231.44	75.24
RAL21	−2360.65	−2387.8	235.33

Table 2. Total energy (ET in Hartree) and dipole moment, drug raltegravir (RAL) and integrase inhibitor analogs.

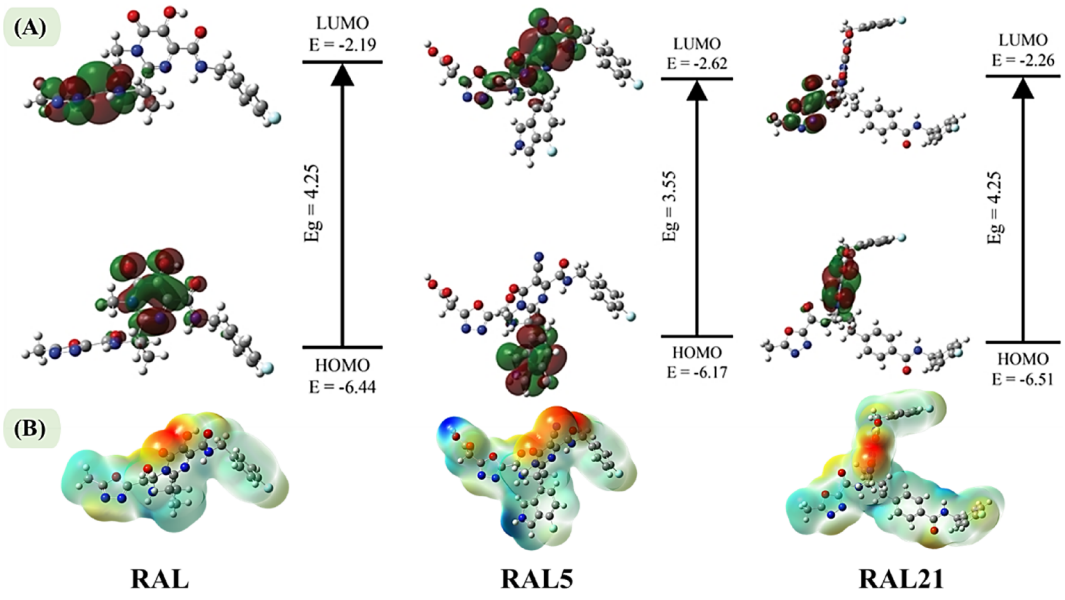

Fig. 3. (**A**) 3D optimized structure and frontier orbital diagrams and (**B**) molecular electrostatic potential of RAL, RAL5 and RAL21 analogs.

indicates the maximum negative region, desirable for electrophilic attack, the blue color indicates the maximum positive region, desirable for nucleophilic attack, and the green color indicates the potential zero region.

Molecular docking simulations

The computation results for binding energy and inhibitory constants clearly indicate that the inhibitors RAL5 and RAL21 exhibit a stronger inhibitory tendency against the HIV-IN protein compared to the inhibitor RAL. These findings suggest that RAL5 and RAL21 may be considered potent inhibitors for reducing the activity of the HIV-IN protein. Docking parameters, including binding energy, inhibitory constant, and intermolecular

Compound	EHOMO(eV)	ELUMO(eV)	Eg(eV)	μ(eV)	η(eV)	S(eV-1)	ω(eV)
RAL	−6.44	−2.19	4.25	−4.31	2.12	0.23	4.38
RAL1	−6.42	−1.73	4.69	−4.07	2.34	0.21	3.54
RAL2	−6.97	−2.66	4.31	−4.81	2.15	0.23	5.37
RAL3	−6.97	−2.68	4.29	−4.82	2.14	0.23	5.42
RAL4	−6.73	−2.98	3.75	−4.85	1.87	0.26	6.28
RAL5	−6.17	−2.62	3.55	−4.39	1.77	0.28	5.44
RAL6	−4.23	−3.47	0.76	−3.85	0.38	1.31	19.5
RAL7	−4.04	−3.64	0.4	−3.84	0.2	2.5	36.86
RAL8	−5.6	−2.59	3.01	−4.09	1.5	0.33	5.57
RAL9	−6.93	−3.84	3.09	−5.38	1.54	0.32	9.38
RAL10	−7.09	−4.3	2.79	−5.69	1.39	0.35	11.62
RAL11	−6.33	−2.87	3.46	−4.6	1.73	0.28	6.11
RAL12	−5.95	−2.46	3.49	−4.2	1.74	0.28	5.06
RAL13	−5.04	−2.1	2.94	−3.57	1.47	0.34	4.33
RAL14	−6.81	−2.97	3.84	−4.89	1.92	0.26	6.22
RAL15	−7.25	−4.41	2.84	−5.83	1.42	0.35	11.96
RAL16	−5.82	−2.62	3.2	−4.22	1.6	0.31	5.56
RAL17	−6.97	−2.67	4.3	−4.82	2.15	0.23	5.4
RAL18	−6.97	−2.65	4.32	−4.81	2.16	0.23	5.35
RAL19	−6.82	−2.28	4.54	−4.55	2.27	0.22	4.56
RAL20	−6.9	−3.61	3.29	−5.25	1.64	0.3	8.39
RAL21	−6.51	−2.26	4.25	−4.38	2.12	0.23	4.52

Table 3. Calculated quantum chemical parameters for raltegravir and designed analogues. μ = Chemical potential, η = Chemical hardness, S = Chemical softness, ω = Electrophilic index.

energy, for the RAL derivatives and the proposed drugs, are reported in Table 4. It is noteworthy that both designed analogs, RAL5 and RAL21, have managed to achieve better energy compared to the original drug (RAL), which is why they have been further investigated through molecular dynamics simulations for a more in-depth evaluation.

According to the results, RAL demonstrates multiple hydrophobic interactions with residues Phe100(B), Ala86(B), Glu87(B), Tyr99(B), Tyr99(A), Glu96(A), Glu87(A), Ala86(A), Phe100(A), Glu85(A), Arg107(A) and Lys103(A), and 2 hydrogen bonds with a distance of 2.64Å and 2.71Å with the residue Lys103(B), and 1 hydrogen bond with a distance of 3.14Å with the residue Arg107(B) in the subunit P31, as shown in Fig. 4A. The designed compound, RAL5, exhibits several hydrophobic interactions with residues Glu96(A), Val88(B), Lys173(B), Tyr99(A), Glu96(B), Tyr99(B), Gln95(B), His171(A), Lys173(A), Thr174(A), Glu87(A), Lys103(B), Phe100(B), Glu87(B), and forms 2 hydrogen bonds with a distance of 2.55Å and 3.01Å with the residue Arg107(A), and 2 hydrogen bonds with a distance of 3.10Å and 2.85Å with the residue Arg107(B), and 1 hydrogen bond with a distance of 2.89Åwith the residue Lys103(A), and also a hydrogen bond with a distance of 2.60Å with the residue Val88(A) in the subunit P31, as illustrated in Fig. 4B. The designed analog, RAL21, also displays multiple hydrophobic interactions with residues Val88(B), Glu85(B), Glu96(B), Lys173(A), Thr125(B), Ala98(B), His171(A), Gln95(B), Tyr99(B), Phe100(B), Glu87(B), Arg107(B), Lys103(B), Lys103(A), Ile89(B), and forms 1 hydrogen bond with a distance of 2.32Å with the residue Thr174(A), and 1 hydrogen bond with a distance of 2.74Å with the residue Lys173(B) in the subunit P31, as depicted in Fig. 4C.

These results indicate that the designed analogs particularly RAL5 and RAL21 not only have lower binding energies but also exhibit stronger interactions with key residues in the active site of the HIV-1 Integrase enzyme. Accordingly, it can be hypothesized that these compounds inhibit the enzyme's activity through multiple simultaneous mechanisms. First, the presence of keto-hydroxy groups in the drug structure likely facilitates the chelation of divalent metal ions (such as Mg^{2+}) at the enzyme's active site, which are essential for its catalytic activity[46,47]. Second, the formation of stable hydrogen bonds with amino acids such as Arg107, Lys103, and Val88 may disrupt the active conformation of the enzyme while enhancing the stability of its inactive form. Third, these interactions may hinder the enzyme's association with other components of the pre-integration complex, ultimately preventing the transfer of viral DNA into the host cell genome[48]. Altogether, these interactions could explain the stronger inhibitory performance of RAL5 and RAL21 compared to Raltegravir.

Molecular dynamics simulations

Molecular dynamics simulations were employed to analyze and investigate the inhibitory effects of RAL and designed drugs on HIV-IN enzymes in more detail. The results obtained from analyses of drug Root Mean Square Deviation (RMSD) at the binding site, protein Cα atom Root Mean Square Fluctuation (RMSF), hydrogen bonds between HIV-IN and the drug, distance calculation, and the number of contacts between the drug and the protein, principal component analysis, as well as active site residues and gyration radii of the enzymes, are

Drug name	BE (kcal/mol)	BE (Redock)	KI (nM&μM)	KI (Redock)	IE (kcal/mol)	IE (Redock)	Refrence RMSD	Refrence RMSD (Redock)
RAL	**−8.38**	**−7.99**	**724.97nM**	**1.39 μm**	**−10.45**	**−10.08**	**7.6**	**3.76**
RAL1	−8.72	−8.23	405.05nM	933.38 nM	−10.81	−10.31	5.91	5.7
RAL2	−8.86	−8.68	321.83nM	431.98 nM	−10.65	−10.47	5.87	6.03
RAL3	−8.98	−8.7	262.43nM	422.88 nM	−11.66	−11.38	6.29	5.95
RAL4	−8.41	−9	679.63nM	251.32 nM	−11.1	−11.69	6.34	6.31
RAL5	**−10.1**	**−9.97**	**39.76nM**	**49.53 nM**	**−13.08**	**−12.95**	**5.9**	**6.09**
RAL6	−9.35	−8.57	139.48nM	520.00 nM	−11.74	−10.96	7.03	4.93
RAL7	−7.87	−8.47	1.72 μm	622.97 nM	−11.15	−11.75	5.46	5.23
RAL8	−8.81	−7.88	351.19nM	1.67 μm	−12.68	−11.76	4.93	5.13
RAL9	−9.04	−7.86	236.26nM	1.74 μm	−13.22	−12.03	4.69	5.49
RAL10	−9.58	−9.6	95.72nM	92.35 nM	−12.86	−12.88	5.96	6
RAL11	−7.44	−7.7	3.51 μm	2.27 μm	−11.62	−11.88	4.53	5.2
RAL12	−8.88	−9.39	310.061nM	131.18 nM	−12.76	−13.27	6.57	6.47
RAL13	−8.46	−9.3	632.91nM	152.13 nM	−11.14	−11.99	4.63	4.73
RAL14	−8.38	−9.44	719.01nM	120.41 nM	−11.66	−12.72	6.76	6.25
RAL15	−8.64	−9.93	463.96nM	52.51 nM	−11.62	−12.91	4.86	6.26
RAL16	−7.83	−8.1	1.822nM	1.16 μm	−11.71	−11.97	5.04	4.81
RAL17	−7.98	−8.27	1.41 μm	873.41 nM	−10.97	−11.25	4.53	4.41
RAL18	−8.55	−8.4	543.59nM	698.08 nM	−12.13	−11.98	4.77	4.78
RAL19	−7.09	−7.45	6.36 μm	3.49 μm	−11.56	−11.92	5.16	5.19
RAL20	−8.93	−9.03	286.80nM	241.61 nM	−12.51	−12.61	4.32	4.28
RAL21	**−10.92**	**−10.43**	**9.95nM**	**22.72 nM**	**−14.79**	**−14.31**	**4.42**	**3.27**

Table 4. Binding energy (BE in kcal/mol), inhibition constant (Ki in nM&pM) and intermolecular energy (IE in kcal/mol) of drugs docked with HIV-IN.

presented in this section. Furthermore, all analyses were performed using Python version 3.12, and the results were visualized in the form of charts and graphs.

MD simulation plays a significant role in examining structural stability, flexibility, spatial changes, and understanding ligand–protein interactions. In the present study, dynamic simulations of the HIV-IN/RAL, HIV-IN/RAL5, and HIV-IN/RAL21 complexes were conducted over a period of 250 nanoseconds. The results showed that the RAL-RAL21 complex reached stability after approximately 60 ns, with an average RMSD of 0.27 nanometers. In contrast, the introduction of the RAL5 analog reduced the RMSD to 0.24 nanometers, indicating stronger interactions and increased complex stability during the simulation (Fig. 5A). Furthermore, RMSF analysis for the RAL5 complex revealed that the binding of this inhibitor did not alter the overall flexibility of the enzyme's active site, but it did result in increased local stability. These results, along with a higher number of hydrogen bonds between RAL5 and key residues such as Arg107(A), Arg107(B), Lys103(A), and Val88(A), clearly demonstrate that this analog has stronger interactions compared to RAL (Fig. 5B). Comparing the results of this study with previous research further supports their validity. In a study by Chitongo et al. (2020), the impact of resistance mutations such as G140S, Y143R, and E92Q on the binding of Dolutegravir to the HIV-IN enzyme was investigated. They found that these mutations led to increased RMSD and decreased structural stability of the complex, ultimately reducing the drug's efficacy. In contrast, the RAL5 analog in the present study successfully maintained structural stability in the absence of mutations, indicating greater resistance to structural instability[49]. Another study by Johnson et al. (2012) emphasized the relationship between the structural stability of integrase inhibitors and their biological activity. They demonstrated that inhibitors with lower RMSD values and more stable hydrogen bonds during simulations also performed better in laboratory settings[50]. Our findings support this correlation, particularly for RAL5, which showed enhanced inhibitory potential compared to the parent drug through reduced RMSD and sustained hydrogen bonding.

By analyzing the number of hydrogen bonds between the ligand and the protein, the degree of association and interaction between these two can be illustrated. The number of hydrogen bonds between the ligand and the protein (for each complex) has been calculated. According to the results, the number of hydrogen bonds between the HIV-IN enzyme and RAL5 is specified to be 1–4 bonds, indicating more interactions compared to RAL and RAL21, as indicated in Fig. 6A.

Secondary structure analysis of the HIV-IN enzyme, through the calculation of the radius of gyration (Rg) and principal component analysis (PCA), provides detailed insights into spatial variations and the flexibility of the protein structure. In this study, the average Rg value for the HIV-IN/RAL and HIV-IN/RAL5 complexes was found to be 1.80 nanometers, indicating overall structural stability of the enzyme in the presence of these two ligands (Fig. 6B). Additionally, PCA results confirmed this stability by revealing no significant changes in the protein's collective motions. In contrast, the RAL21 complex exhibited less stable values in both Rg and PCA analyses, suggesting a reduction in dynamic coordination and increased atomic dispersion within the enzyme

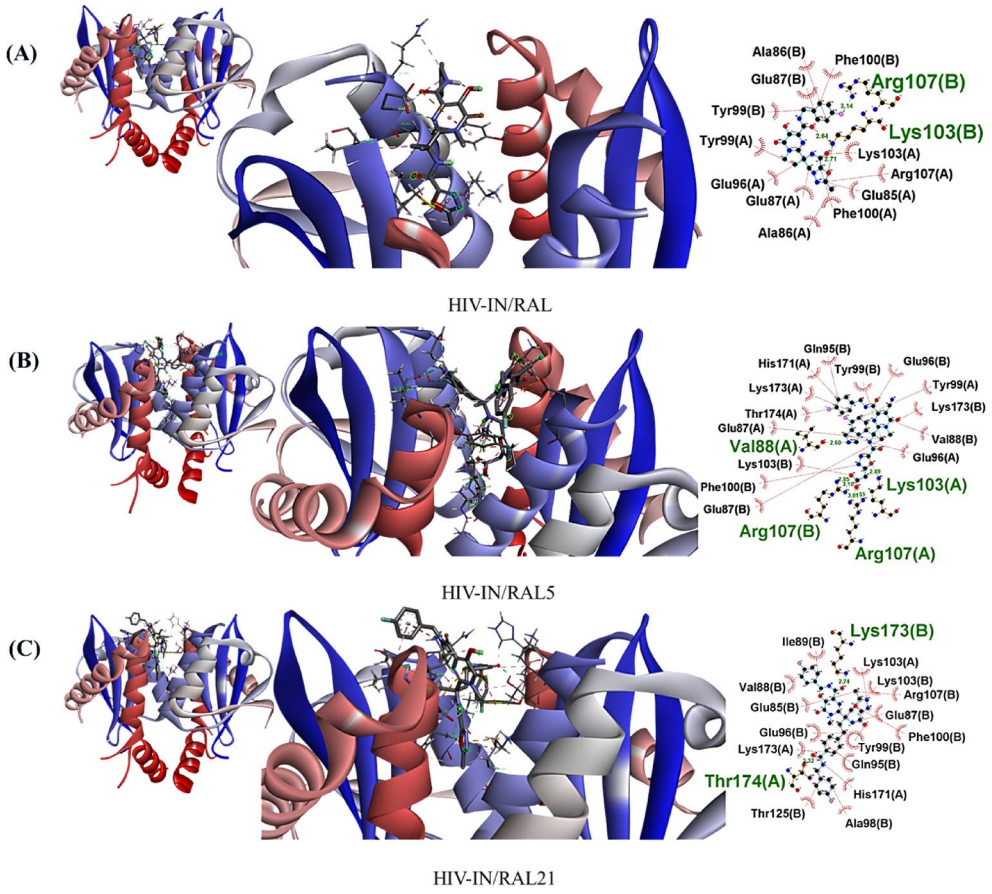

Fig. 4. Hydrogen bonding and hydrophobic interactions of (**A**) RAL, (**B**) RAL5 and (**C**) RAL21 with the amino acids of HIV-IN binding site.

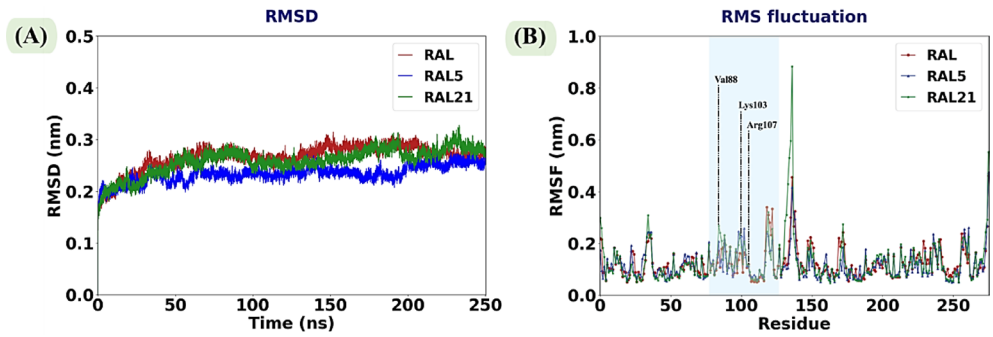

Fig. 5. (**A**) RMSD and (**B**) RMSF of Cα atoms of HIV-IN residues in HIV-IN/RAL (red), HIV-IN/RAL5 (blue), and HIV-IN/RAL21 (green) complexes.

structure (Fig. 6C). The findings from the Rg and PCA analyses are consistent with previous reports on the role of stable complexes in maintaining protein structural integrity. For instance, Sun et al. demonstrated that inhibitors with more uniform molecular mass distribution and reduced PCA fluctuations exhibit more stable secondary structures and optimized dynamic behavior in biological environments an observation clearly evident in the case of the RAL5 analo. Similarly, the study by Chitongo et al. emphasized that increased Rg values and irregular PCA patterns can be indicative of protein structural instability in the presence of weaker or mutated inhibitors, a feature observed for RAL21[51].

For a better understanding of the interactions between the protein and the drug, the number of contacts between these two entities has been calculated. At the initial stage of the simulation, the number of contacts between HIV-IN/RAL-RAL5-RAL21 is shown in Fig. 6D. As the simulation progresses, the number of contacts for IN/RAL5 increases compared to the original drug. To confirm the analysis of the number of contacts, Fig. 6E

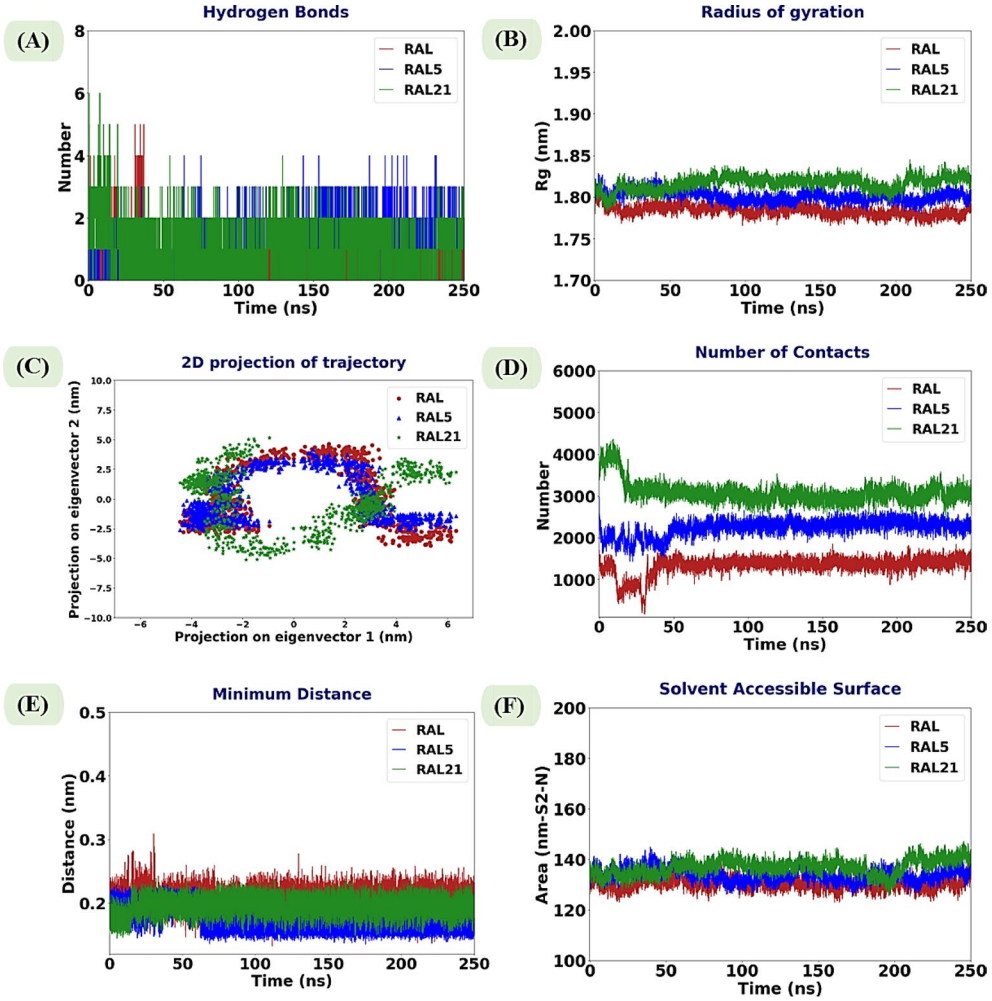

Fig. 6. (**A**) Number of hydrogen bonds, (**B**) radius of gyration of Cα atoms, (**C**) PCA analysis, (**D**) number of contacts, (**E**) minimum distance and (**F**) solvent accessible surface diagram in HIV-IN/RAL (red), HIV-IN/RAL5 (blue) and HIV-IN/RAL21 (green), complexes.

depicts the distance between the protein and drugs during the 250 nanoseconds of simulation. According to this plot, a constant value is observed over the 250 nanoseconds for IN/RAL-RAL5-RAL21, indicating an optimal distance between the protein and drugs. These results clearly demonstrate that the designed drug has a greater ability to inhibit the integrase enzyme compared to the RAL drug.

Our findings are consistent with the results of Sun et al. (2023), who demonstrated that an increased number of stable contacts between a drug and its target enzyme during dynamic simulations is directly associated with enhanced drug efficacy and stronger enzyme inhibition. From this perspective, the RAL5 analog by maintaining an optimal distance and gradually increasing the number of molecular contacts exhibited better inhibitory performance compared to Raltegravir and can be considered a more potent inhibitor[52].

Additionally, the solvent-accessible surface area (SASA) is a vital parameter in studying the three-dimensional structure of proteins, structural changes, and understanding their interactions with other molecules such as ligands or proteins. As illustrated in Fig. 6F, a portion of the surface of IN/RAL, which is not accessible to solvent molecules, is located in the protein core and often associated with the hydrophobic core of the protein. On the other hand, IN/RAL5-RAL21, which is entirely accessible to solvent molecules, implies effective interaction of the integrase enzyme with the designed drugs (RAL5-RAL21).

In a study by Sun et al., it was emphasized that an increase in solvent-accessible surface area (SASA) and a reduction in protein structural compactness in the presence of more effective inhibitors are directly associated with enhanced drug–target interactions and greater complex stability[53]. Accordingly, the SASA analysis results for RAL5, alongside other dynamic findings, position it as a candidate with higher inhibitory potential and greater structural stability compared to Raltegravir features that support its potential as a next-generation drug for inhibiting the HIV-1 integrase enzyme.

Prediction of pharmacokinetic and drug-likeness properties

To more accurately assess the drug-like potential of the designed compounds, all analogs, along with the reference drug Raltegravir (RAL), were subjected to ADMET property prediction analyses. This evaluation was

conducted using the ADMETlab 2.0 database to provide a comprehensive insight into their pharmacokinetic properties, toxicity, absorption, metabolism, and elimination profiles. The results indicated that, in addition to their favorable performance in quantum chemical calculations, molecular docking, and molecular dynamics simulations, the designed compounds also exhibit promising drug-like characteristics. The RAL5 analog, with an appropriate molecular weight (616.16 Da), very low blood–brain barrier (BBB) penetration (0.001), longer half-life (T½ = 0.831), and high plasma protein binding (PPB = 97.65%), is recognized as a compound with considerable systemic stability. Furthermore, its high topological polar surface area (TPSA = 208.89 Å²) and moderately balanced LogP value (0.633) indicate an optimal balance between water solubility and membrane permeability. On the other hand, RAL21, with higher lipophilicity (LogP = 2.486), lower polarity (TPSA = 181.34 Å²), and greater BBB penetration (0.004), shows promising potential for the development of targeted therapies within the central nervous system (CNS). Although it has a shorter half-life compared to RAL5, its absorption and distribution properties are suitable for specialized pharmaceutical forms, such as brain-targeted drug delivery. Notably, all designed compounds particularly RAL5 and RAL21 adhere to the principles of rational drug design. They comply with Lipinski's Rule of Five, including appropriate molecular weight, LogP under 5, acceptable numbers of hydrogen bond donors and acceptors, and suitable polarity. Additionally, the design of these analogs also takes into account the Pfizer rule, which focuses on minimizing hepatotoxicity and improving absorption and bioavailability. The synthetic accessibility (SA) score analysis further reveals that despite their relatively more complex structures compared to the reference drug, both RAL5 and RAL21 remain within an acceptable range for laboratory and industrial-scale synthesis. In summary, the results of this analysis highlight RAL5 as the leading candidate for preclinical studies and final drug formulation, due to its balanced profile in terms of stability, safety, bioavailability, and full compliance with drug design principles. Meanwhile, RAL21 emerges as a promising option for CNS-focused therapeutic applications (Table 5).

Binding free energy calculations

As presented in Table 6, in investigated systems, van der Waals interactions, electrostatic, and nonpolar solvation energies are quite favorable for binding the inhibitor to HIV-IN. The binding free energy of HIV-IN/RAL, HIV-IN/RAL5 and HIV-IN/RAL21 complexes were calculated for 250 snapshots acquired from the last 20 ns of the trajectories. The total binding free energy, ΔGbind, for HIV-IN/RAL5 is more favorable than HIV-IN/RAL.

Gibbs free energy landscape (FEL) analysis

The Free Energy Landscape (FEL) was generated using a mesh map and various color patterns such as red, yellow, orange, blue, etc., to analyze the maximum and minimum energy levels of the HIV-IN/RAL, HIV-IN/RAL5, and HIV-IN/RAL21 complexes. As shown in Fig. 7, the HIV-IN/RAL5 complexes exhibit more stable compounds compared to HIV-IN/RAL and HIV-IN/RAL21. The drug complexes HIV-IN/RAL, HIV-IN/RAL5, and HIV-IN/RAL21 also displayed Gibbs free energy values ranging from 0 to 16 kilojoules per mole. Furthermore, 3D FEL plots of the HIV-IN/RAL, HIV-IN/RAL5, and HIV-IN/RAL21 complexes were generated to determine the Root Mean Square Deviation (RMSD) and Radius of Gyration (Rg) for the optimal complex conformation. As

Compounds	Chemical Formula	Molecular weight	Density	Flexibility	PPB	BBB Penetration	Pgp-inhibitor	SA score	Log *P*	TPSA	T 1/2
Ral	C20H21 FN6O5	444.16	1.061	0.4	88.31%	0.018	0.026	2.871	0.728	152.24	0.45
Ral1	C20H22 FN7O4	443.17	1.054	0.4	92.89%	0.035	0.006	3.024	1.085	154.89	0.574
Ral2	C21H21 FN8O3	452.17	1.04	0.381	93.17%	0.035	0.009	3.153	0.911	158.45	0.572
Ral3	C26H24 FN9O4	545.19	1.039	0.407	91.33%	0.052	0.013	3.232	0.608	181.58	0.605
Ral4	C24H21 FN10O5	548.17	1.075	0.333	92.91%	0.103	0.009	4.368	0.229	224.69	0.736
Ral5	C29H22 F2 N8O6	616.16	1.071	0.344	97.65%	0.001	0.003	4.039	0.633	208.89	0.831
Ral6	C26H22 FN11O6	603.17	1.091	0.312	75.61%	0.005	0.026	5.196	−0.078	256.3	0.299
Ral7	C29H27 ClFN13O6	707.19	1.106	0.343	93.49%	0.03	0	5.378	−0.17	304.84	0.316
Ral8	C29H24 F2 N8O8	650.17	1.092	0.406	95.49%	0.001	0.004	4.117	0.383	248.42	0.643
Ral9	C24H22 FN11O9	627.16	1.128	0.4	80.89%	0.005	0	4.604	−2.024	316.52	0.788
Ral10	C26H22 FN11O7	619.17	1.091	0.367	90.89%	0.003	0.001	4.278	−0.186	287.22	0.753
Ral11	C32H26 F2 N10O8	716.19	1.083	0.412	97.07%	0.001	0	4.764	0.09	291.93	0.647
Ral12	C34H31 F2 N9O6	699.24	1.053	0.351	98.89%	0.005	0.008	4.453	0.625	217.97	0.76
Ral13	C33H27 F2 N11O3	663.23	1.041	0.297	97.20%	0.022	0.185	4.396	1.704	200.02	0.748
Ral14	C27H21 FN12O5	612.17	1.079	0.333	78.03%	0.674	0.032	4.696	−0.284	250.47	0.611
Ral15	C29H24 FN13O5	653.2	1.07	0.314	92.67%	0.055	0.004	4.338	0.204	275.7	0.636
Ral16	C30H23 FN10O9	686.16	1.09	0.382	94.64%	0.001	0.001	4.579	−0.697	315.3	0.743
Ral17	C25H22 FN11O5	575.18	1.074	0.379	96.16%	0.021	0.004	4.108	−0.634	247.29	0.766
Ral18	C26H21 FN10O8	620.15	1.097	0.4	84.85%	0.004	0	4.346	−1.579	281.94	0.744
Ral19	C28H23 FN12O9	690.17	1.114	0.361	85.49%	0.044	0.001	4.601	−1.466	326.78	0.751
Ral20	C24H22 FN11O8	611.16	1.117	0.414	93.65%	0.043	0.014	4.464	−0.453	286.87	0.411
Ral21	C35H33 F2 N7O6	685.25	1.026	0.455	100.59%	0.004	0.989	3.594	2.486	181.34	0.216

Table 5. Scrutiny of physicochemical properties of RAL compounds and designed analogues.

Free Energies (kJ/mol)	RAL	RAL5	RAL21
van der Waal energy	−68.368	−73.148	−63.393
Electrostattic energy	−6.654	−30.36	−21.056
Polar solvation energy	74.444	114.328	103.209
SASA energy	−9.262	−20.944	−30.078
Binding energy	−9.84	−10.142	−11.319

Table 6. Free energies of HIV-IN/RAL, HIV-IN/RAL5 and HIV-IN/RAL21 complexes calculated by MMPBSA (energies in kcal/mol).

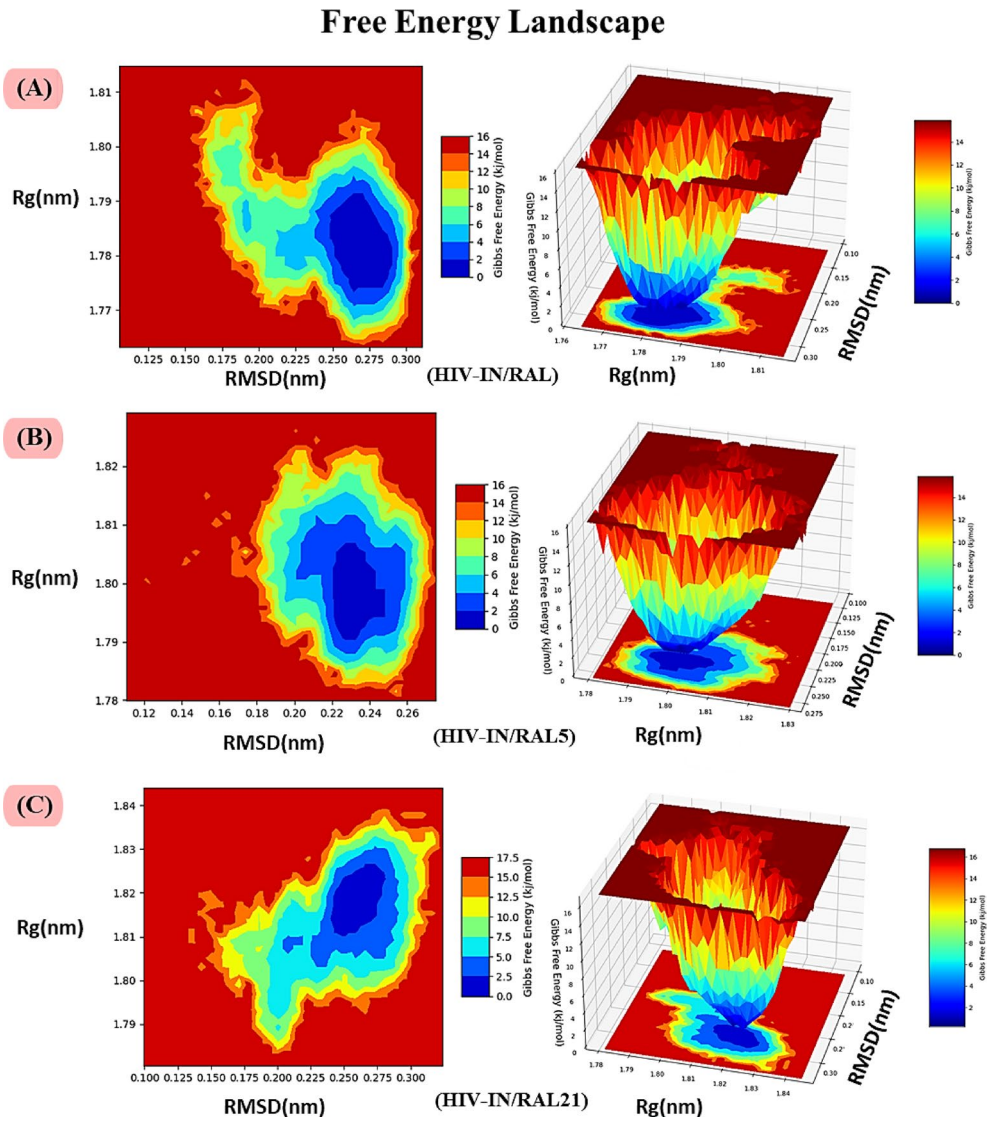

Fig. 7. A graphical representation of the Gibbs free energy (FEL) landscape of the complexes: HIV-IN/RAL(**A**), HIV-IN/RAL5(**B**), and HIV-IN/RAL21(**C**), obtained from a molecular dynamics simulation study.

shown in Fig. 7, the HIV-IN/RAL5 complex exhibited lower values of RMSD and Rg (Rg = 1.78, RMSD = 0.23) in comparison to the HIV-IN/RAL complex (Rg = 1.785, RMSD = 0.265) and the HIV-IN/RAL21 complex (Rg = 1.817, RMSD = 0.255). The results obtained from the free energy landscape indicate that the HIV-IN/RAL5 complexes are more stable than the other complexes. Consequently, FEL analysis shows that when ligands are properly bound, the protein folds into its lowest energy state. Moreover, the FEL of these complexes reveals deep basins in regions with higher free energy. Dark blue regions indicate local minimum energy states that actively promote stable conformations.

Conclusion

In summary, Structure-Based Drug Design is a logical approach that successfully utilizes structural information from HIV-IN to design drug molecules competitively binding to a specific target, such as Raltegravir. A chemical library of 21 compounds with structural similarity to Raltegravir was created. The retrieved compounds were further analyzed and optimized at two computational levels, Hartree-Fock and B3LYP using the 6-311G basis set. Additionally, calculations related to frontier orbitals were performed to illuminate reactivity in these configurations. Furthermore, for a better understanding of the electrophilic and nucleophilic regions of drugs, crucial for drug transport, electronic potential calculations were carried out using more precise computational methods. Molecular docking was carried out to perform quantitative and qualitative analyses on the interactions of candidate molecules within the active site. Among all compounds, RAL5 and RAL21 exhibited binding energies of −10.1 kcal/mol and − 10.92 kcal/mol, respectively, indicating a stronger inhibitory nature against the HIV-IN enzyme compared to RAL, which had a binding energy of −8.38 kcal/mol. Simulations of RAL, RAL5 and RAL21 in the HIV_IN protein were conducted. Finally, MD simulation analyses, including RMSD and RMSF, were conducted, demonstrating greater structural stability of RAL5 compared to RAL and RAL21 throughout the simulation (duration: 250 ns). Moreover, by connecting the inhibitor RAL5, it could establish stronger hydrogen bonds. Measurement of distances and the number of contacts between drugs and proteins showed that HIV-IN/RAL5 performs better in inhibiting the HIV-IN enzyme compared to the primary drugs. Additionally, a comparison of Rg and PCA revealed that the increase in surface amino acids by RAL5 leads to an expansion of the protein radius and a reduction in protein density. Furthermore, SASA analysis showed that the HIV-IN/RAL5 complex, which had access to the solvent compared to the drug RAL, exhibited more effective interactions with the HIV-IN enzyme. Collectively, these parameters contribute to the most comprehensive understanding of the behavior and interactions within these molecular biological systems.

Data availability

The data are available from the corresponding author, upon reasonable request.

Received: 4 January 2025; Accepted: 7 May 2025
Published online: 13 May 2025

References

1. Kleinberg, M. L. & Wanke, L. A. New approaches and technologies in drug design and discovery. *Am. J. Health Syst. Pharm.* **52** (12), 1323–1336 (1995).
2. Duarte, Y. et al. Integration of target discovery, drug discovery and drug delivery: a review on computational strategies. *Wiley Interdisciplinary Reviews: Nanomed. Nanobiotechnol.* **11** (4), e1554 (2019).
3. Najafi, V., Yoosefian, M. & Hassani, Z. Development of venetoclax performance using its new derivatives on BCL-2 protein Inhibition. *Cell Biochem. Funct.* **41** (1), 58–66 (2023).
4. Yoosefian, M., Moghani, M. Z. & Juan, A. In silico evaluation of atazanavir as a potential HIV main protease inhibitor and its comparison with new designed analogs. *Comput. Biol. Med.* **145**, 105523 (2022).
5. Bour, S., Geleziunas, R. & Wainberg, M. A. The human immunodeficiency virus type 1 (HIV-1) CD4 receptor and its central role in promotion of HIV-1 infection. *Microbiol. Rev.* **59** (1), 63–93 (1995).
6. Engelman, A. & Cherepanov, P. The structural biology of HIV-1: mechanistic and therapeutic insights. *Nat. Rev. Microbiol.* **10** (4), 279–290 (2012).
7. Su, M., Tan, J. & Lin, C. Y. Development of HIV-1 integrase inhibitors: recent molecular modeling perspectives. *Drug Discovery Today*. **20** (11), 1337–1348 (2015).
8. Esposito, D. & Craigie, R. HIV integrase structure and function. *Adv. Virus Res.* **52**, 319–333 (1999).
9. Popov, S. et al. Viral protein R regulates nuclear import of the HIV-1 pre-integration complex. *EMBO J.* **17** (4), 909–917 (1998).
10. Stanic, M. *Epi-genomic determinants of HIV-1 integration in primary CD4 + T cells and macrophages*. (2020).
11. Trivedi, J. et al. Recent advances in the development of integrase inhibitors for HIV treatment. *Curr. HIV/AIDS. Rep.* **17**, 63–75 (2020).
12. Maertens, G. N., Engelman, A. N. & Cherepanov, P. Structure and function of retroviral integrase. *Nat. Rev. Microbiol.* **20** (1), 20–34 (2022).
13. Engelman, A. N. Multifaceted HIV integrase functionalities and therapeutic strategies for their Inhibition. *J. Biol. Chem.* **294** (41), 15137–15157 (2019).
14. Mohamed, H. et al. Targeting CCR5 as a component of an HIV-1 therapeutic strategy. *Front. Immunol.* **12**, 816515 (2022).
15. Paparizos, V. & Kourkounti, S. *HIV Infection and AIDS: the Present Status of Antiretroviral therapy, in European Handbook of Dermatological Treatments*p. 429–442 (Springer, 2023).
16. Elliott, J. L. & Kutluay, S. B. Going beyond integration: the emerging role of HIV-1 integrase in virion morphogenesis. *Viruses* **12** (9), 1005 (2020).
17. Barski, M. S., Minnell, J. J. & Maertens, G. N. Inhibition of HTLV-1 infection by HIV-1 first-and second-generation integrase strand transfer inhibitors. *Front. Microbiol.* **10**, 1877 (2019).
18. De Castro, N. *Efficacy of raltegravir-based Regimens for Antiretroviral Treatment of People with HIV and Tuberculosis in low-and middle-income Countries: Insight from Clinical Trials* (Université de Bordeaux, 2022).
19. Ugbe, F. A. et al. Computational evaluation of the inhibitory potential of some Urea, thiourea, and Selenourea derivatives of diselenides against leishmaniasis: 2D-QSAR, pharmacokinetics, molecular docking, and molecular dynamics simulation. *J. Mol. Struct.* **1302**, 137473 (2024).
20. Ugbe, F. A. et al. Cheminformatics-based discovery of new organoselenium compounds with potential for the treatment of cutaneous and visceral leishmaniasis. *J. Biomol. Struct. Dynamics*. **42** (24), 13830–13853 (2024).
21. Edache, E. I. et al. Drug-like screening, molecular docking, molecular dynamics simulations, and binding free energies on the interaction of pyrazole derivatives as inhibitors of lysosomal storage disorders and anticancer activity. *Discover Chem.* **1** (1), 22 (2024).
22. Edache, E. I. et al. *DFT studies on structure, electronics, bonding nature, NBO analysis, thermodynamic properties, molecular docking, and MM-GBSA evaluation of 4-methyl-3-[2-(4-nitrophenyl)-1, 3-dioxo-2, 3-dihydro-1 H-isoindole-5-amido] benzoic acid: a potent inhibitor of Graves' disease.* Journal of Umm Al-Qura University for Applied Sciences, : pp. 1–19. (2024).
23. Ugbe, F. A. et al. Cheminformatic evaluation of the multi-protein binding potential of some diselenide derivatives: A plausible drug discovery approach for leishmaniasis. *Discover Chem.* **1** (1), 25 (2024).

24. Edache, E. I. et al. Evaluation of novel Anti-SARS-CoV-2 compounds by targeting nucleoprotein and envelope protein through homology modeling, Docking simulations, ADMET, and molecular dynamic simulations with the MM/GBSA calculation. *Intell. Pharm.* **2** (3), 346–366 (2024).
25. Goodsell, D. S. et al. RCSB protein data bank: enabling biomedical research and drug discovery. *Protein Sci.* **29** (1), 52–65 (2020).
26. Iwaniak, A. et al. Characteristics of biopeptides released in Silico from collagens using quantitative parameters. *Foods* **9** (7), 965 (2020).
27. Shao, Q. & Zhu, W. Assessing AMBER force fields for protein folding in an implicit solvent. *Phys. Chem. Chem. Phys.* **20** (10), 7206–7216 (2018).
28. Basha, F. et al. Computational evaluation on molecular structure (Monomer, Dimer), RDG, ELF, electronic (HOMO-LUMO, MEP) properties, and spectroscopic profiling of 8-Quinolinesulfonamide with molecular docking studies. *Comput. Theor. Chem.* **1198**, 113169 (2021).
29. Frisch, M. et al. *Gaussian 16* (Gaussian, Inc. Wallingford, 2016).
30. Hussein, H. A. et al. PockDrug-Server: a new web server for predicting pocket druggability on holo and Apo proteins. *Nucleic Acids Res.* **43** (W1), W436–W442 (2015).
31. Yoosefian, M., Moghani, M. Z. & Juan, A. Silico evaluation of Atazanavir as a potential HIV main protease inhibitor and its comparison with new designed analogs. *Comput. Biol. Med.* **145**, 105523 (2022).
32. Ross, B. J. *A Lamarckian Evolution Strategy for Genetic Algorithms, in Practical Handbook of Genetic Algorithms*p. 1–16 (CRC, 2019).
33. Seeliger, D. & de Groot, B. L. Ligand Docking and binding site analysis with PyMOL and Autodock/Vina. *J. Comput. Aided Mol. Des.* **24** (5), 417–422 (2010).
34. Laskowski, R. A. & Swindells, M. B. *LigPlot+: Multiple ligand–protein Interaction Diagrams for Drug Discovery* (ACS, 2011).
35. DeLano, W. L. *Pymol: An open-source molecular graphics tool.* CCP4 Newsl. *Protein Crystallogr.* **40** (1), 82–92 (2002).
36. Vanommeslaeghe, K. et al. CHARMM general force field: A force field for drug-like molecules compatible with the CHARMM all-atom additive biological force fields. *J. Comput. Chem.* **31** (4), 671–690 (2010).
37. Mark, P. & Nilsson, L. Structure and dynamics of the TIP3P, SPC, and SPC/E water models at 298 K. *J. Phys. Chem. A.* **105** (43), 9954–9960 (2001).
38. Harrach, M. F. & Drossel, B. *Structure and dynamics of TIP3P, TIP4P, and TIP5P water near smooth and atomistic walls of different hydroaffinity*. *J. Chem. Phys.*, **140**(17). (2014).
39. Price, D. J. & Brooks, C. L. A modified TIP3P water potential for simulation with Ewald summation. *J. Chem. Phys.* **121** (20), 10096–10103 (2004).
40. Xiong, G. et al. ADMETlab 2.0: an integrated online platform for accurate and comprehensive predictions of ADMET properties. *Nucleic Acids Res.* **49** (W1), W5–W14 (2021).
41. Xue, W. et al. What contributes to serotonin–norepinephrine reuptake inhibitors' dual-targeting mechanism? The key role of transmembrane domain 6 in human serotonin and norepinephrine transporters revealed by molecular dynamics simulation. *ACS Chem. Neurosci.* **9** (5), 1128–1140 (2018).
42. Wang, P. et al. Differentiating physicochemical properties between NDRIs and sNRIs clinically important for the treatment of ADHD. *(BBA)-General Subj.* **1861** (11), 2766–2777 (2017). Biochimica et Biophysica Acta.
43. Kumari, R. et al. g_mmpbsa A GROMACS tool for high-throughput MM-PBSA calculations. *J. Chem. Inf. Model.* **54** (7), 1951–1962 (2014).
44. Gohlke, H., Kiel, C. & Case, D. A. Insights into protein–protein binding by binding free energy calculation and free energy decomposition for the Ras–Raf and Ras–RalGDS complexes. *J. Mol. Biol.* **330** (4), 891–913 (2003).
45. Kagami, L. P. et al. Geo-Measures: A PyMOL plugin for protein structure ensembles analysis. *Comput. Biol. Chem.* **87**, 107322 (2020).
46. Hare, S. et al. Structural and functional analyses of the second-generation integrase strand transfer inhibitor dolutegravir (S/GSK1349572). *Mol. Pharmacol.* **80** (4), 565–572 (2011).
47. Pommier, Y., Johnson, A. A. & Marchand, C. Integrase inhibitors to treat HIV/AIDS. *Nat. Rev. Drug Discovery*. **4** (3), 236–248 (2005).
48. Popov, S. et al. *Viral Protein R Regulates Nuclear Import of the HIV-1 pre-integration Complex* (The EMBO journal, 1998).
49. Chitongo, R. et al. Molecular dynamic simulations to investigate the structural impact of known drug resistance mutations on HIV-1 C Integrase-Dolutegravir binding. *PLoS One*. **15** (5), e0223464 (2020).
50. Johnson, B. C. et al. Molecular dynamics approaches estimate the binding energy of HIV-1 integrase inhibitors and correlate with in vitro activity. *Antimicrob. Agents Chemother.* **56** (1), 411–419 (2012).
51. Li, M. et al. Mechanisms of HIV-1 integrase resistance to dolutegravir and potent Inhibition of drug-resistant variants. *Sci. Adv.* **9** (29), eadg5953 (2023).
52. Wang, Y. C. et al. The discovery of Indole-2-carboxylic acid derivatives as novel HIV-1 integrase strand transfer inhibitors. *Molecules* **28** (24), 8020 (2023).
53. Sun, Q. et al. *Elucidating the molecular determinants of the binding modes of a Third-Generation HIV-1 integrase strand transfer inhibitor: the importance of side chain and solvent reorganization*. *Viruses*, **16**(1). (2024).

Acknowledgements
The authors wish to thank Graduate University of Advanced Technology, Kerman, Iran, for their support.

Author contributions
H.S.: Methodology, Visualization, Writing - Review & Editing; M.Y.: Conceptualization, Methodology, Formal analysis. All authors read and approved the final manuscript.

Funding
Not applicable.

Declarations

Competing interests
The authors declare no competing interests.

Additional information
Correspondence and requests for materials should be addressed to M.Y.